HHS Public Access

Author manuscript

*Nat Cell Biol*. Author manuscript; available in PMC 2017 March 19.

Published in final edited form as:

*Nat Cell Biol*. 2016 October ; 18(10): 1031–1042. doi:10.1038/ncb3411.

# iPSC-derived cardiomyocytes reveal abnormal TGFβ signaling in left ventricular non-compaction cardiomyopathy

**Kazuki Kodo**[1,2], **Sang-Ging Ong**[1,2], **Fereshteh Jahanbani**[3], **Vittavat Termglinchan**[1,2,4], **Keiichi Hirono**[6], **Kolsoum InanlooRahatloo**[1,2], **Antje D. Ebert**[1,2,4], **Praveen Shukla**[1,2], **Oscar J. Abilez**[1,2], **Jared M. Churko**[1,2,4], **Ioannis Karakikes**[1,2,4], **Gwanghyun Jung**[1,5], **Fukiko Ichida**[6], **Sean M. Wu**[1,2], **Michael P. Snyder**[3], **Daniel Bernstein**[1,5,*], and **Joseph C. Wu**[1,2,4,*]

[1]Stanford Cardiovascular Institute, Stanford University School of Medicine

[2]Department of Medicine, Division of Cardiology, Stanford University School of Medicine

[3]Department of Genetics, Stanford University School of Medicine

[4]Institute of Stem Cell Biology and Regenerative Medicine, Stanford University School of Medicine

[5]Department of Pediatrics, Stanford University School of Medicine

[6]Department of Pediatrics, University of Toyama

## Abstract

Left ventricular non-compaction (LVNC) is the third most prevalent cardiomyopathy in children and its pathogenesis has been associated with the developmental defect of the embryonic myocardium. We show that patient-specific induced pluripotent stem cell-derived cardiomyocytes (iPSC-CMs) generated from LVNC patients carrying a mutation in the cardiac transcription factor TBX20 recapitulate a key aspect of the pathological phenotype at the single-cell level and was associated with perturbed transforming growth factor beta (TGFβ) signaling. LVNC iPSC-CMs have decreased proliferative capacity due to abnormal activation of TGFβ signaling. TBX20 regulates the expression of TGFβ signaling modifiers including a known genetic cause of LVNC, PRDM16, and genome editing of PRDM16 caused proliferation defects in iPSC-CMs. Inhibition



*Correspondence: Joseph C. Wu, Lorry Lokey Stem Cell Building, 265 Campus Drive G1120B, Stanford, CA 94305-5454. joewu@stanford.edu or danb@stanford.edu.

**COMPETING FINANCIAL INTERESTS**

The authors declare no competing financial interests.

**Referenced accessions**

RNA-sequencing: GSE63161

Exome-sequencing: Variant Analysis; URL: https://variants.ingenuity.com/Jahanbani2016, SRA reference; SRP080041.

**AUTHOR CONTRIBUTIONS**

All authors have read and approved the manuscript. K.K., S.-G.O., D.B. and J.C.W. designed research, performed the experiments and wrote the manuscript; F.I., D.B. and J.C.W. recruited the patients; K.K., J.M.C., and S.-G.O. generated and performed experiments on iPSCs/ESCs with the help of A.D.E. and G.J.; K.K., F.J., K.H., K.I. and J.M.C. performed sequencing and bioinformatics analysis; S.M.W. generated NK-TGCK transgenic mouse; K.K., V.T. and I.K. generated genome-corrected iPSC lines; K.K., P.S. and O.J.A. performed and interpreted the patch clamping and calcium imaging data; M.P.S. provided scientific advice; and J.C.W. provided funding and supervised the entire research project.

of TGFβ signaling and genome correction of the TBX20 mutation were sufficient to reverse the disease phenotype. Our study demonstrates that iPSC-CMs are a useful tool for the exploration of pathological mechanisms underlying poorly understood cardiomyopathies including LVNC.

## Introduction

Left ventricular non-compaction (LVNC) is increasingly recognized as a cause of cardiomyopathy[1, 2], especially in children. In a recent study, LVNC accounted for 9.2% of all children with primary cardiomyopathies, and was the third most prevalent form of cardiomyopathy, after dilated cardiomyopathy (DCM) and hypertrophic cardiomyopathy (HCM)[2]. LVNC is characterized by deep and extensive hypertrabeculation of the left ventricle, and causes heart failure, arrhythmias, and thromboembolism.

LVNC has been theorized to result from the arrest of compaction of the developing LV myocardium, as it passes through several distinct evolutionally conserved steps. Trabeculations in the human embryo emerge after looping of the primitive heart tube at the end of the fourth week of gestation[3]. Trabecular remodeling begins at 8 weeks with an increase in LV volume compressing the trabeculations, leading to an increase in thickness of the compacted myocardium. Serial pathologic studies suggest that LVNC arises from impaired/arrested compaction of the myocardium, abnormalities of vascularization, or in development of the multilayered spiral system[3, 4]. Among these steps, emergence of trabeculations and trabecular remodeling are thought to be the key steps to understanding LVNC. The trabeculation patterns are ventricle-specific, which are generally thicker and the corresponding intertrabecular spaces are larger in the LV than in the right ventricle. When this embryonic pattern persists postnatally, the morphologic appearance strongly resembles the embryonic “spongiform” myocardium, which was the original nomenclature for this cardiomyopathy.

Like many congenital cardiomyopathies, the genetics of LVNC is complex and the full spectrum of the disorder is still undefined. The mechanisms that lead to LVNC are not well understood, although animal models of LVNC have suggested that abnormal regulation of growth signals, including the transforming growth factor beta (TGFβ)[5–9], NOTCH, and NRG1/ERBB2[10, 11], may be causative factors. Since most of these animal models harboring non-compaction-like myocardium showed alterations in cell cycle regulation in developing cardiomyocytes, it is thought that the abnormal proliferation of embryonic cardiomyocytes may be associated with the pathogenesis of LVNC. However, studies have differed on whether this proliferation is increased or decreased[5–7, 9]. Furthermore, recent human studies have identified mutations in genes which are associated with regulation of cardiomyocyte proliferation[11, 12]. However, it is still unclear which phenotypes in developing cardiomyocytes are actually associated with the pathogenesis seen in humans and investigation of this disease has been challenging due to its complex genetic basis.

To overcome the problems for the investigation of human cardiac cell development with pathological background of LVNC, we used patient-specific induced pluripotent stem cells (iPSCs). Here we demonstrated the use of human iPSC-derived cardiomyocytes (iPSC-CMs)

from patients carrying the TBX20 mutation affected by LVNC as a model to define cell-specific phenotypes and elucidate potential mechanisms of this disease.

## Results

### TBX20 mutation is a candidate genetic cause of LVNC

To identify potential genetic causes of LVNC, we recruited a family with LVNC including the proband #1 (A-III-4), who had undergone heart transplantation for restrictive physiology, two siblings (A-III-2 and A-III-3) with significantly deeper and more extensive trabeculation of the left ventricle (a form-fruste of LVNC referred to clinically as "hypertrabeculation") but with normal systolic function, and the father (A-II-2) with asymptomatic dilated cardiomyopathy (DCM) without LVNC (Figs. 1a–c and Supplementary Table 1). Genetic testing by genome-wide exome sequencing revealed a stop-gain mutation in the TBX20 gene (Y317*) in the proband #1, two siblings, and father (Fig. 1d). No mutations in maternally-transmitted and *de novo* modifiers known to contribute to cardiomyopathies were detected (Supplementary Table 2). To investigate whether TBX20 mutations are seen in other LVNC patients, we performed genetic testing in an additional 77 LVNC patients and detected another *de novo* mutation (T262M) from one additional isolated LVNC patient (proband #2: B-II-2) (Figs. 1a, 1b, 1d and Supplementary Table 1).

TBX20 is an essential cardiac transcription factor that regulates cardiomyocyte differentiation and proliferation[13, 14]. TBX20 has also been described in conjunction with congenital heart disease[15–17] and DCM[18, 19]. The TBX20 Y317* mutation resulted in a truncated protein (Fig. 1e). TBX20 Y317* and T262M mutant proteins showed disturbed synergistic activity with other cardiac transcription factors, including NKX2-5, GATA4, and TBX5 (Supplementary Figs. 1a and 1b). Furthermore, both TBX20 Y317* and T262M mutations were found to impair the negative transcriptional regulatory function of TBX20 compared to wild-type (Supplementary Fig. 1c). These results suggest that LVNC-associated mutations caused disturbance of transcriptional regulation by TBX20.

### LVNC iPSC-CMs possess a defect of proliferative capacity

To investigate the pathological mechanism of LVNC, we generated iPSCs using Sendai virus reprogramming from a family with LVNC history along with three unrelated control volunteers[20, 21]; two clones per patient were established (Supplementary Figs. 1d–f and Supplementary Table 3). We classed all lines into three subgroups: unrelated control, mild DCM (A-II-2), and LVNC (A-III-2, 3, 4). iPSCs were differentiated into cardiomyocytes (iPSC-CMs)[22], followed by glucose deprivation to enrich for iPSC-CMs (Supplementary Fig. 2a)[23]. Although LVNC iPSC-CMs were similar to control iPSC-CMs in terms of structural and electrophysiological phenotype as well as sarcomeric gene expression at 2–4 weeks, LVNC iPSC-CMs showed approximately 50% reduction of the expression of TBX20 downstream target genes compared with control iPSC-CMs (Fig. 1f, Supplementary Figs. 2b–j and Supplementary Table 4). Furthermore, the differentiation efficiency was also halved in LVNC iPSC lines compared to the control prior to glucose deprivation (Fig. 1g). On the other hand, mild DCM iPSC-CMs showed intermediate defects in TBX20 target gene expressions and differentiation efficiency between LVNC and control iPSC-CMs. Despite

comparable expression of mesodermal markers including MESP1 and brachyury (T) across all lines during cardiac differentiation (Supplementary Fig. 2k), LVNC iPSCs had significantly lower expression of cardiac transcription factors compared to control cell lines especially between day 6 and 9 (Fig. 1h and Supplementary Fig. 3a). These results suggest an impaired induction of cardiac lineage from mesodermal progenitors in LVNC iPSCs.

Since past human and mouse studies have shown possible association between cell-cycle defects in developing cardiomyocytes and pathogenesis of LVNC[5–7, 12, 24], we next assessed the proliferative potential in iPSC-CMs. We found that iPSC-CMs were responsive to growth factors and had increased numbers within 3 weeks after induction of differentiation although their growth was temporary (Supplementary Fig. 3b). In order to assess the proliferation potential in developing iPSC-CMs, distribution of S-phase cardiomyocytes was validated by EdU incorporation with or without stimulation of serum or growth factors. LVNC iPSC-CMs showed reduced baseline proliferative capacity by ~50% without any stimulation as well as in the presence of serum and growth factors compared to control cells at an earlier time point (2 weeks), whereas mild DCM iPSC-CMs showed a milder reduction of ~30% compared to control (Figs. 1i and 1j). On the other hand, undifferentiated iPSCs showed no significant difference in their growth speed (Supplementary Fig. 3c), suggesting the proliferation defect may be characteristic in differentiated cardiac cells.

## Abnormal activation of TGFβ signaling is associated with proliferation defect in LVNC iPSC-CMs

To clarify potential signaling pathways associated with the proliferation defect in LVNC iPSC-CMs, we next performed RNA-sequencing using control, mild DCM, and LVNC iPSC-CMs at 2 weeks. Upstream regulator analysis predicted that activation of TGFβ signaling may be potentially responsible for this differential gene expression between control and LVNC iPSC-CMs (Fig. 2a, Supplementary Fig. 4a and Supplementary Table 5). Most of the TGFβ signaling pathway, especially TGFβ1 associated genes, were upregulated in LVNC and mild DCM iPSC-CMs compared to control iPSC-CMs (Fig. 2b and Supplementary Figs. 4b and 4c). Previous studies have shown that aberrant TGFβ signaling causes incomplete compaction of myocardium in mice[6, 9], and that TGFβ signaling inhibits proliferation of embryonic cardiomyocytes[25, 26] via upregulation of cyclin-dependent kinase inhibitors (CKI) including CDKN1A[27–29]. Consistent with these studies, LVNC iPSC-CMs showed significant upregulation of TGFβ signaling-related genes and 1.7-fold higher phosphorylation of SMAD2/3 (Fig. 2c and Supplementary Figs. 4d and 4e), whereas mild DCM iPSC-CMs had less phosphorylation (1.2-fold vs control). LVNC iPSC-CMs also showed a 1.8-fold increased CDKN1A expression compared to control iPSC-CMs (Fig. 2d and Supplementary Figs. 4f and 4g), suggesting that activation of the TGFβ1-CDKN1A regulatory axis may be responsible for the early cell cycle exit seen in LVNC iPSC-CMs. Histological analysis of proband's explanted LV myocardium revealed higher phosphorylation of SMAD2 in comparison to control LV tissue, providing further evidence of activated TGFβ signaling as a pathogenesis of LVNC (Fig. 2e). Interestingly, LVNC iPSC-CMs showed significantly higher expression of TGFβ signaling pathway associated genes compared to mild DCM iPSC-CMs that were associated with milder phenotypic severity (Supplementary Figs. 4b–g).

In order to understand the difference in disease severity between the father (mild DCM phenotype) and his children (LVNC phenotype), despite carrying the same TBX20 mutation, we next assessed expression of the mutant TBX20 allele by RNA-sequencing and digital droplet PCR. We found that the ratio of mutant allele against wild-type allele expression was higher in LVNC iPSC-CMs than in mild DCM iPSC-CMs (Fig. 2f), suggesting a dosage effect of the TBX20 mutant allele on the ectopic activation level of the TGFβ signaling pathway in patient-specific iPSC-CMs and perhaps explaining for the differences in phenotypic severity among affected family members. In order to confirm that stimulation with TGFβ isoforms could affect the proliferation potential in iPSC-CMs, we treated control iPSC-CMs with TGFβ isoforms with or without serum or growth factors. We found that, like LVNC iPSC-CMs, TGFβ-treated control iPSC-CMs showed a significant decrease of proliferative response to serum, IGF-1, and IGF-2 stimulation at 2 weeks compared to TGFβ-untreated control iPSC-CMs (Fig. 2g). These results suggest that activation of TGFβ signaling has a negative effect on the proliferative potential of developing cardiomyocytes.

## Ectopic activation of TGFβ signaling causes a cardiomyocyte proliferation defect *in vivo*

To assess how abnormal TGFβ1 signaling affects myocardial development *in vivo*, we next generated cardiac-specific TGFβ1 overexpression transgenic mice ($\beta1^{glo}$/αMHC-Cre; Supplementary Figs. 5a and 5b). These double-transgenic mice exhibit embryonic lethality by embryonic day (E) 11.5 due to decreased proliferation in developing cardiomyocytes (Figs. 3a–d, and Supplementary Figs. 5c and 5d, and Supplementary Table 6), providing further proof implicating aberrant TGFβ signaling in the embryonic heart with developmental arrest of the compact layer.

Next, in order to assess the later stages of compact layer development, we crossed $\beta1^{glo}$ transgenic mice with NK-TGCK transgenic mice that express GFP-Cre fusion protein under the control of the Nkx2-5 cardiac-specific enhancer/promoter and Tet-Off system to negatively regulate GFP-Cre expression upon doxycycline (DOX) exposure (Supplementary Fig. 5e). The αMHC-Cre transgene labeled >90% of cardiomyocytes at E12.5 and the NK-TGCK transgene activated Cre in ~40% of cardiomyocytes without DOX and ~25% of cardiomyocytes with DOX treatment and showed significantly lesser TGFB1 mRNA expression compared to αMHC-Cre/$\beta1^{glo}$ double transgenic mouse embryos at E10.5 (Supplementary Figs. 5f–h). The double transgenic embryos carrying both NK-TGCK and $\beta1^{glo}$ ($\beta1^{glo}$/NK-TGCK) without DOX treatment showed significant increase of TGFβ downstream target genes whereas the double transgenic embryos with DOX treatment showed only mild increase of these genes at E10.5 (Supplementary Fig. 5i). The $\beta1^{glo}$/NK-TGCK double transgenic embryos showed embryonic lethality around E12.5 to E13.5. In contrast, when mice were treated with DOX, the embryos could survive normally at E12.5 (Fig. 3e and Supplementary Table 7). Histological analysis showed a significantly thinner compact layer and reduced Ki67 or phospho-histone H3 (PHH3)-positive cardiomyocytes in the compact layer in $\beta1^{glo}$/NK-TGCK double transgenic embryos without DOX compared to wild-type litter mates, although the trabecular layer was well developed in these double transgenic embryos (Figs. 3f–h and Supplementary Figs. 5j and 5k). Half of DOX-treated $\beta1^{glo}$/NK-TGCK double transgenic embryos showed reduced thickness of the LV compact layer, and the proportion of $Ki67^{+}$ or $PHH3^{+}$ cardiomyocytes in the compact layer in

β1$^{glo}$/NK-TGCK embryos was mildly decreased compared to wild-type littermates (Figs. 3f, 3i and 3j, and Supplementary Figs. 5j and 5k).

To assess the fate of TGFβ1-activated CMs in DOX-treated transgenic mice, we next generated triple transgenic embryos carrying NK-TGCK/β1$^{glo}$ transgenes with Cre-dependent tdTomato overexpression system (Ai14)[30]. We found that the proportion of TGFβ1-activated CMs in LV was significantly decreased in triple transgenic embryos and neonates during development compared to control (NK-TGCK/Ai14) mice, suggesting reduced proliferation by TGFβ-expressing CMs (Figs. 4a and 4b). Furthermore, the hearts of triple transgenic neonates at postnatal day 3 showed thicker trabecular layer and thinner compact layer resulting in significantly higher non-compaction/compaction (NC/C) ratio in LV myocardium compared to control neonates (Figs. 4c–e). Taken together, these results support the role of abnormal activation of TGFβ signaling to cause developmental arrest of cardiomyocytes in a temporal and dose-dependent manner *in vivo*.

## Functional disturbance of TBX20 causes abnormal activation of TGFβ signaling

Next, to assess whether the defective TBX20 transcriptional cascade causes abnormal activation of TGFβ signaling, we analyzed the gene expression profile of the Tbx20 knockout mouse[31]. Interestingly, mRNA expression analysis of Tbx20 knockout mouse heart revealed a similar gene expression profile to that of LVNC iPSC-CMs, including upregulation of TGFβ signaling (Fig. 5a and Supplementary Table 8)[31]. Furthermore, ChIP-sequencing data of Tbx20[31] showed conserved TBX20 binding sites in the genes that are associated with TGFβ signaling regulation and modification between human and mouse (Fig. 5b and Supplementary Table 9). This gene expression profile was significantly disturbed in LVNC iPSC-CMs compared to control iPSC-CMs, as well as in the Tbx20 knockout mouse heart compared to wild-type (Fig. 5c and 5d). We further employed shRNA against TBX20 in H7 human embryonic stem cell (ESC) line (TBX20KD-H7) (Figs. 6a and 6b), and found that TBX20KD-H7-CMs showed less proliferative capacity and increased expression of TGFβ–related genes compared with scramble control lines (Figs. 6c–g). These results confirm that the dysfunction of TBX20 is associated with the pathological proliferation phenotype of LVNC iPSC-CMs through disturbance of the TGFβ signaling.

## TBX20-PRDM16 axis regulates TGFβ signaling and contributes to cardiomyocyte proliferation

To better understand the regulatory mechanism of TGFβ signaling by TBX20, we next studied TGFβ modifiers with conserved TBX20 binding sites[31] between human and mouse (Supplementary Table 9), and selected PRDM16 gene as one of the potential downstream targets of TBX20. PRDM16, a repressor of TGFβ signaling and known genetic cause of LVNC and DCM, was significantly downregulated in all LVNC iPSC-CMs, TBX20KD-H7-CMs, and the Tbx20 knockout mouse heart (Figs. 5d, 6h and 6i). A previous genetic study of human LVNC with the PRDM16 mutation also revealed that truncation in exon 9 of PRDM16 is associated with LVNC phenotype[12]. To confirm whether LVNC iPSC-CMs with the PRDM16 mutation showed abnormal activation of TGFβ signaling and a proliferation defect, as seen in LVNC iPSC-CMs with the TBX20 mutation, we next generated genome-edited iPSC line carrying the frameshift mutation in exon 9 of the PRDM16 gene

(PRDM16fs) and induced cardiac differentiation (Fig. 6j). Importantly, PRDM16fs iPSC-CMs showed significantly decreased proliferative response when exposed to growth factors and upregulation of TGFβ downstream target genes (Figs. 6k and 6l). Furthermore, the explanted heart tissue of proband #1 showed a significant decrease of PRDM16 expression compared to control donor heart tissue (Fig. 6m), suggesting the TBX20-PRDM16-TGFβ axis as one of the mechanisms causing LVNC.

### Modification of TGFβ signaling or genetic correction of the TBX20 mutation exacerbate the proliferation defect in LVNC iPSC-CMs

Finally, we evaluated whether modification of aberrant TGFβ signaling could rescue the proliferation defect in LVNC iPSC-CMs. Inhibition of TGFβ signaling with TGFβ receptor-1 inhibitors or overexpression of dominant negative form of TGFβ receptor-2 increased S-phase cells in both LVNC iPSC-CMs and TBX20KD-H7-CMs compared to untreated cells (Figs. 7a-c and Supplementary Figure 6). Likewise, knockdown of the downstream effector, CDKN1A, also improved the distribution of S-phase LVNC iPSC-CMs (Figs. 7d–f). To validate the effects of the TBX20 Y317* mutation on the phenotype of LVNC iPSC-CMs, we generated TBX20 Y317* mutation-corrected (LVNC-corrected) iPSCs from the proband's iPSCs (Supplementary Figs. 7a–e). LVNC-corrected iPSC-CMs showed increased cardiac differentiation efficiency, expression of cardiac transcription factors, and restored proliferative capacity compared to non-corrected LVNC iPSC-CMs along with decreased TGFβ signaling activity (Figs. 7g–k). These results suggest that the TBX20 mutation contributes to the pathological phenotype of LVNC iPSC-CMs via disturbance of TGFβ signaling, which is associated with developmental defects of the compact layer during embryogenesis (Supplementary Fig. 7f).

## Discussion

Previously, both accelerative[9, 11] and decelerative proliferation[5–7, 12] in embryonic cardiomyocytes have been reported in animal models. In our transgenic mouse model, high overexpression of TGFB1 in the developing myocardium led to a severe developmental arrest in the compact layer and the severity of this non-compaction phenotype was directly correlated with the levels of TGFB1 overexpression. These observations suggest that at the early developmental stage of LV compact layer remodeling, proper activation of TGFβ signaling in the embryonic heart is required to ensure normal ventricular development.

Human iPSC-CMs have been used to model familial dilated cardiomyopathy[23, 32, 33], familial hypertrophic cardiomyopathy[34, 35], long QT syndrome[36–38], among others[39]. In this study, we demonstrate that iPSC-CM technology is useful not only for delineating the detailed molecular pathogenesis of congenital developmental defects, but also to clarify genetic causes in such diseases. We successfully found an association between functional disturbance of TBX20 and ectopic activation of TGFβ signaling in patient-specific iPSC-CMs as well as perturbed regulation of putative downstream targets of TBX20. We showed that PRDM16 is a possible downstream target gene of TBX20. PRDM16 is a known cause of LVNC in humans and morpholino knockdown of PRDM16 causes a proliferation defect in the developing zebrafish heart[12]. PRDM16 is a repressor of TGFβ signaling[40–42] via

binding of SMAD2/3, and our results revealed ectopic activation of TGFβ signaling in LVNC iPSC-CMs consistent with these previous studies. Although the comprehensive RNA expression data and ChIP-sequencing data showed that TBX20 has a large number of potential downstream target genes associated with TGFβ signaling regulation, our data suggests that the TBX20/PRDM16/TGFβ signaling pathway may be one of the key regulatory cascades for proper development of the compact/trabecular layer.

It is known that patients with LVNC generally show a wide spectrum of clinical manifestations. Some are asymptomatic, and the age at presentation can vary considerably, from as early as the newborn period to as late as older adulthood[43, 44]. This may be explained by varying expression levels of mutant allele-specific mRNA expression between mild DCM and LVNC as shown here. TBX20 is known to interact with other cardiac transcription factors including NKX2-5, GATA4, and TBX5 that are essential for embryonic cardiomyocyte proliferation and ventricular development. As shown here, the disturbance of interaction between TBX20 and these cardiac transcription factors may negatively impact the expansion of embryonic cardiomyocytes and impair the formation of the multilayered compact myocardium (Supplementary Fig. 7f). The differences of allele-specific TBX20 expression and the background expression of these cardiac transcription factors which may also be affected by heterogeneous factors could then impact the various cardiac phenotypes in patients with TBX20 mutations.

In conclusion, iPSC-CMs recapitulate the proliferative defects associated with LVNC[5–7, 12] at the single cell level. Importantly, this study presents the supporting evidence of a proliferation defect, a consequence of abnormal activation of TGFβ signaling, as a pathological feature of human LVNC. Whether this defect is common to all cases of LVNC or just a genetic subset remains to be determined. Our data suggest that iPSC-CMs may be useful in therapeutic screening to identify potential interventions for this cardiomyopathy in the future.

## Methods

### Derivation of human induced pluripotent stem cells (iPSCs)

Fibroblasts or peripheral blood mononuclear cells (PBMCs) were obtained from family members with LVNC with informed consent under protocols approved by the Stanford University Human Subjects Research Institutional Review Board. Human skin-punch biopsies were digested with Collagenase II and transferred into 6-well culture dish (BD Biosciences). At passage 2 or later, primary fibroblasts were used for reprogramming to iPSCs using the non-integrating Sendai virus-based CytoTune™-iPS Reprogramming Kit (Life Technologies). After 24 h and 72 h, the medium was replaced. At day 4, cells were detached using TrypleE (Life Technologies) and replated onto mouse embryonic fibroblasts (MEF)-coated 6-well plates in DMEM/Glutamax with 10% FBS and Rho-associated, coiled-coil containing protein kinase (ROCK) inhibitor, Y27632 (Selleckchem). From day 5 onwards, cells were cultured in mTeSR medium (STEMCELL Technologies). Colonies were picked after day 20 and transferred to a Matrigel-coated culture dish (BD Biosciences), and subsequently passaged using Accutase (Global Cell Solutions). After passage 10, culture medium was changed to Essential 8 (Life Technologies)[20]. PBMC reprogramming was

performed as described previously[21]. Briefly, PBMCs were isolated using a Ficoll-Paque Premium (GE Healthcare) from 20 ml of whole blood and plated at 1 million cells per milliliter in 2 ml of blood medium[21]. After day 9, $1\times10^6$ cells were plated in blood medium with Sendai virus. Cells were transferred to mTeSR medium in a MEF-coated 6-well plate at day 3. Colonies were picked after day 20 and transferred to a new Matrigel-coated culture dish and cultured as described above.

### Culture and maintenance of iPSCs and ESCs

Human ESCs and iPSCs were grown on Matrigel-coated plates using chemically-defined E8 medium as described before[20]. The medium was changed daily and cells were passaged every 4 days using EDTA.

### Cardiac differentiation

iPSCs were grown to 90% confluence and differentiated subsequently into beating cardiomyocytes, using a small molecule-based monolayer method described in detail previously[22]. Ten days after cardiac differentiation, iPSC-CM monolayers were purified using RPMI-1640 without glucose (Life Technologies) with B27 supplement (Life Technologies). Non-glucose culture medium was changed every 2 days. After 5 days, iPSC-CMs were reseeded onto Matrigel-coated plates in culture medium with glucose.

### Pluripotency marker analysis

Human ESC and iPSC colonies grown in Matrigel-coated 8-well chamber glasses (Thermo Scientific) were fixed using 4% paraformaldehyde (PFA) and permeabilized with 0.5% Triton X-100. After blocking samples with 5% goat serum in PBST (PBS with 0.1% Tween20), cells were stained with mouse anti-SSEA4 (R&D systems), rabbit anti-OCT3/4 (Santa Cruz Biotechnology), rabbit anti-NANOG (Santa Cruz Biotechnology), and mouse anti-TRA1-60 (EMD Millipore) antibodies. Cells were then incubated with AlexaFluor-conjugated secondary antibodies (Life Technologies) and Hoechst 33342 (Life Technologies) to visualize the specific stains. Image acquisition was performed on an Eclipse 80i fluorescent microscope (Nikon Instruments).

### Teratoma formation assay

$1\times10^6$ iPSCs were suspended in 25 μL PBS, mixed with equal volumes of Matrigel, and injected into the subcutaneous regions of the anterior thigh of immunodeficient female SCID mice (n=2 spots per group of mice) (Charles River Laboratories). Fifty days after transplantation, teratomas were explanted, fixed with 4% paraformaldehyde, set in paraffin, sectioned, and stained with hematoxylin & eosin (H&E).

### Plasmid construction and site-directed mutagenesis

The Flag-tagged Human TBX20 expression vector (TBX20-pCMV tag2B), GATA4 expression vector (GATA4-pcDNA3.1), NKX2.5 expression vector (NKX2.5-pcDNA3.1), TBX5 expression vector (TBX5-pcDNA3.1), and the NPPA promoter luciferase reporter vector (NPPA-pGL3 basic) were kindly provided by Hiroyuki Yamagishi. Site-directed mutagenesis was performed using a QuikChange Site-Directed Mutagenesis Kit (Agilent

Technologies) according to the manufacturer's instructions. The MSX2 promoter sequence containing a 3.9-kb fragment of the MSX2 5′ untranslated and franking region was subcloned into pGL3-Basic (Promega), as described previously[45]. All constructed vectors were verified by sequencing.

### Luciferase assay

The HeLa cells were purchased from ATCC. The cells were not authenticated or tested for mycoplasma contamination recently. No cell lines used in this study were found in the database of commonly misidentified cell lines that is maintained by ICLAC and NCBI Biosample. HeLa cells were transfected using Lipofectamine 2000 (Life Technologies) with 50 ng reporter vector, 50 ng expression vectors, and 0.2 ng pRL-SV40 internal control vector (Promega). Luciferase activity was measured 48 h after transient transfection by using Dual-Glo Luciferase Reporter Assay System (Promega) according to the manufacturer's instructions. Two duplicate, six independent assays were performed.

### Immunocytochemistry

Cells grown on cover slips were fixed using 4% PFA, permeabilized with 0.5% Triton X-100, incubated with primary antibodies and Hoechst 33342, and detected using Alexa Fluor conjugated secondary antibodies. Primary antibodies used include mouse anti-FLAG M2 (Sigma Aldrich), rabbit anti-cardiac troponin T (Abcam), mouse anti-cardiac troponin T (Thermo Scientific), mouse anti-sarcomeric alpha-actinin (Sigma Aldrich), or rabbit anti-TBX20 (Abcam), as published previously[45]. Image acquisition was performed on an Eclipse 80i fluorescent microscope and a confocal microscope (Carl Zeiss, LSM 510 Meta) and ZEN software (Carl Zeiss). Measurement of cell surface area and length was performed using NIS-Elements Basic Research 3.0 software (Nikon). A detailed list for antibodies used is shown in Supplementary Table 10.

### EdU-based proliferation analysis

iPSC-CMs were cultured in RPMI with B27 supplement and 2% FBS 2 days prior to EdU staining to accelerate the proliferation. Staining was performed using the Click-it EdU Imaging Kit (Life technologies) according to the manufacturer's instructions. EdU was incorporated for 24 h prior to experiment. Cells were fixed with 4% PFA, permeabilized with 0.5% TritonX-100 in PBS, and stained with Alexa Fluor-conjugated azide. After washing and blocking with 5% goat serum in PBST, cells were incubated with a rabbit anti-TNNT2 antibody (Abcam) and visualized with anti-rabbit Alexa Fluor-conjugated secondary antibody and Hoechst 33342. At least more than one hundred cells were counted per sample and more than three independent studies per group were performed. Measurement of the fluorescent signals was performed using NIS elements BR analysis 4.13.04 64-bit software (Nikon).

### RNA sequencing

Eight paired-end cDNA libraries (two biological replicates of proband iPSC-CMs, two biological replicates of father iPSC-CMs, one biological replicate of two sibling iPSC-CMs, and one biological replicate of two control iPSC-CMs) were prepared and sequenced. Total

RNA was extracted and quantified using miRNeasy Kit (Qiagen) according to the manufacturer's protocol. 10 μg of total RNA was used to generate index-tagged paired-end cDNA libraries. Briefly, mRNAs were purified by polyA enrichment procedure using Dynal Oligo(dT) beads (Life technologies). mRNA fragmentation was performed using RNA Fragmentation Reagents (Life technologies) to obtain 200–300 bp fragments. cDNA was generated using SuperScript Double-Stranded cDNA Synthesis Kit (Life technologies). Illumina sequencing adapters were ligated to cDNA using LigaFast (Promega) and PE Adapter Oligo Mix (Illumina, San Diego, CA). PCR was performed on the adapter-ligated cDNA with 2X Phusion DNA polymerase Master Mix (New England Biolabs, Ipswich, MA). Sequencing was performed with Illumina's HiSeq2000 or 2500 platform using paired end reads at an average length of 100 bps (2×100).

## RNA-seq data processing and differential expression analysis

Paired-end fastq sequence reads from each sample were assembled against hg19 using the Tophat v2.0.6 (http://tophat.cbcb.umd.edu) with the Illumina-supplied hg19 gene-model annotation file (gtf annotation). The expression level (FPKM, Fragments Per Kilobase of exon per Million fragments mapped) was estimated by Cufflinks (http://cufflinks.cbcb.umd.edu). Q-value is same as false discovery rate. Cuffdiff was used to call differentially expressed genes with a false discovery rate less than 0.05. Cuffdiff was run against the UCSC iGenomes GTF file from Illumina (http://cufflinks.cbcb.umd.edu/igenomes.html). Subsequent to determining which genes were differentially expressed, FPKM was used for filtering and visualization purposes. Only genes with expression values > 1 FPKM in at least one sample were considered for subsequent analysis. Samtools (http://samtools.sourceforge.net/) was used to calculate allele-specific expression of TBX20 gene. We used this software to analyze the differentially expressed genes between controls and LVNC patients. Using IPA Upstream Regulator analysis, the cascade of upstream transcriptional regulators was predicted, and this explained the observed gene expression changes. This upstream regulator analysis is based on prior knowledge of expected effects between transcriptional regulators and their target genes stored in the Ingenuity® Knowledge Base. Activation z-score was validated to infer the activation states of predicted transcriptional regulators by the IPA Upstream Regulator analysis. The *p*-value measures whether there is a statistically significant overlap between the dataset genes and the genes that are regulated by a transcription regulator. The *p*-value calculated using Fisher's Exact Test, and significance is generally attributed to $p < 0.01$. RNA and ChIP-sequencing data of wild-type and Tbx20 knockout mouse heart were obtained from NCBI GEO database (RNA-sequencing: http://www.ncbi.nlm.nih.gov/geo, ChIP-sequencing: http://www.ncbi.nlm.nih.gov/geo/query/acc.cgi?acc=GSM734426)[31]. All of the RNA sequencing data can be accessed as the GEO reference GSE63161 (URL: http://www.ncbi.nlm.nih.gov/geo/query/acc.cgi?token=kdizeyiyzlilpcn&acc=GSE63161).

## Quantifying allele specific expression using RNA-seq data

Allele specific expression of TGFB gene was measured using RNA-Seq data. Alignment was performed using tophat v2.0.6 (http://tophat.cbcb.umd.edu) and processed using SAMtools v0.1.2, which produces site-specific allele frequencies using overlapping reads (read pileup). Allele specific expression was calculated by determining whether or not each

overlapping read at mutant site fitted the reference or the mutant allele. These summed counts represented our measures of relative allelic abundance at that site. Any deviation from equal allelic abundance was reflected as allelic imbalance[46].

### Quantitative RT-PCR

Total RNA was prepared using RNAeasy plus kit (Qiagen). cDNA was synthesized by the High Capacity cDNA Reverse Transcription Kit (Life Technologies). Quantitative real-time polymerase chain reaction (qRT-PCR) was performed on a StepOne Real-Time PCR System (Life Technologies) using the TaqMan Universal PCR Master Mix (Life technologies) according to the manufacturer's protocol. Relative quantification was normalized against GAPDH. More than three respective sets of experiments were performed.

### Digital droplet PCR for the detection and quantification of TBX20 wild-type and mutant allele-specific mRNA

Total RNA of 2 week old LVNC and mild DCM iPSC-CMs were extracted and prepared using RNAeasy plus kit (Qiagen). cDNA was synthesized by the High Capacity cDNA Reverse Transcription Kit (Life Technologies). The quantification of allele specific mRNA expression was analyzed using the QX100 Droplet Digital PCR system (Bio-Rad, Hercules, CA, USA). Y317* mutation was detected with an FAM probe: 5′ FAM-ZCCATCCGTACCTACGGAGGAGAX- Black Hole Quenche 3′, and the wild-type allele with another HEX probe: 5′ HEX-ZCCATCCGTACCTAAGGAGGAGAX- Black Hole Quencher 3′. Each reaction mix consisted of the following: 2x ddPCR Supermix, 20x specific target primers including the forward primer (5′ GGAAAGTGTGGAGAGCCTGA 3′) and the reverse primer (5′ TGACTCTCATCCCCCAAGAC 3′), 20x mutant-specific FAM probes, 20x wild-type-specific HEX-probe, 5 ng cDNA template, and the mixture was adjusted with PCR grade water to a final volume of 20 μl. The thermal cycling conditions were as follows: enzyme activation, 95°C for 10 min (1 cycle); denaturation, 94°C for 30 s (40 cycles); annealing/extension, 61°C for 1 min (40 cycles); and hold 98°C for 10 min (1 cycle). The ddPCR data were analyzed with QuantaSoft analysis software (Bio-Rad), and the quantification of either the deletion or the insertion allele was presented as the number of copies per microliter of PCR mixture.

### Western blotting

Following SDS-PAGE, proteins were transferred to 0.45 μm nitrocellulose membranes (Bio-Rad) using a mini Bio-Rad Mini PROTEAN 3 Cell system in NuPAGE transfer buffer (Life technologies). The membrane was then blocked in Membrane Blocking Solution (Life technologies) and incubated with primary antibody overnight at 4 °C. Blots were incubated with the appropriate secondary antibodies for 1 h at room temperature and visualized using ECL Western Blotting Analysis System (GE Healthcare). Primary antibodies used were biotinylated SMAD2/3 (Cell Signaling), phospho-SMAD2/3 (Cell Signaling), CDKN1A (Cell Signaling), TBX20 (Sigma Aldrich), and HRP conjugated α–Tubulin (Cell Signaling). A detailed list of antibodies used is shown in Supplementary Table 10.

### $Ca^{2+}$ imaging

Briefly, 30 day old iPSC-CMs were dissociated with TrypLE and reseeded on Matrigel-coated 22-mm round coverslips. The Fluo-4 Direct Calcium Assay kit was used (Life Technologies) as per the manufacturer's instructions. Fluo-4 loading solution was incubated with the cells at 37 °C for 30 min and fluorescence was measured at 495±20 nm excitation and 515±20 nm emission. Videos were taken of iPSC-CMs spontaneously beating or electrically field-stimulated at 1 and 2 Hz, 10 V/cm, and 10 ms biphasic pulse width. Measurements were taken on an AxioObserver Z1 inverted microscope (Carl Zeiss) equipped with a Lambda DG-4 300 W Xenon light source (Sutter Instruments), an ORCA-ER CCD camera (Hamamatsu), and AxioVison 4.7 software (Zeiss). All experiments were conducted at 37 °C with normal culture medium (RPMI-1640 with B27 supplement). The mean $Ca^{2+}$ signals of ten paced beats were analyzed with ImageJ software. More than three sets of experiments were performed.

### Patch clamp

Whole cell action potentials were recorded with the use of standard patch-clamp technique, as previously described[22]. Briefly, cultured iPSC-CMs were plated on No. 18 mm glass cover slips (Warner Instruments) coated with Matrigel, placed in a RC-26C recording chamber (Warner Instruments), and mounted onto the stage of an inverted microscope (Nikon, Tokyo, Japan). The chamber was continuously perfused with warm (35–37 °C) extracellular solution (pH 7.4) of following composition: (mM) 150 NaC1, 5.4 KCl, 1.8 $CaCl_2$, 1.0 $MgCl_2$, 1.0 Na pyruvate, 15 HEPES, and 15 glucose. Glass micropipettes were fabricated from standard wall borosilicate glass capillary tubes (Sutter BF 100-50-10, Sutter Instruments) using a programmable puller (P-97; Sutter Instruments) and filled with the following intracellular solution (pH 7.2): 120 KCl, 1.0 $MgCl_2$, 10 HEPES, 10 EGTA, and 3 Mg-ATP. A single beating cardiomyocyte was selected and action potentials (APs) were recorded in whole cell current clamp mode using an EPC-10 patch-clamp amplifier (HEKA). Data were acquired using PatchMaster software (HEKA) and digitized at 1.0 kHz. The following criteria are used for classifying observed APs into ventricular-, atrial-, and nodal-like iPSC-CMs. For ventricular-like, the criteria were a negative maximum diastolic membrane potential (<−50 mV), a rapid AP upstroke, a long plateau phase, AP amplitude > 90 mV, and AP duration at 90% repolarization/AP duration at 50% repolarization (APD90/APD50) < 1.4. For atrial-like, the criteria were an absence of a prominent plateau phase, a negative diastolic membrane potential (<−50 mV), and APD90/APD50 > 1.7. For nodal-like, the criteria were a more positive MDP, a slower AP upstroke, a prominent phase 4 depolarization, and APD90/APD50 between 1.4 and 1.7[22].

### Transgenic mice

αMHC-Cre mice[47], mTmG mice[48], and NK-TGCK mice[49] were previously described. The tdTomato reporter mice (Ai14)[30] and transgenic mice that conditionally express active TGF-β1 upon genomic recombination by Cre recombinase ($\beta1^{glo}$)[50] were purchased from the Jackson Laboratory. All transgenic mice were backcrossed with C57BL6 background more than five times. αMHC-Cre mice and NK-TGCK mice were crossed with mTmG reporter transgenic mice to observe the Cre activity in embryonic heart. αMHC-Cre mice and NK-

TGCK mice were also crossed with $\beta1^{glo}$ mice to obtain cardiac-specific TGFβ1 overexpression (αMHC-Cre/$\beta1^{glo}$ or NK-TGCK/$\beta1^{glo}$) double-transgenic embryos. Doxycycline (2 mg/ml plus 50 mg/ml sucrose) was administrated orally in the drinking water and replaced every 4 days. Pregnant female mice were treated with doxycycline from embryonic day 0.5 to 7.0. For the generation of the NK-TGCK/β1glo double-transgenic adult female mice, pregnant female mice were treated with doxycycline from embryonic day 0.5 to 12.5 to inactivate the NK-TGCK transgene during pregnancy. NK-TGCK/$\beta1^{glo}$ double-transgenic female mice were crossed with Ai14 male mice to obtain triple transgenic embryos and neonates. All experimental procedures were approved by the ethics committee of Stanford University and were in accordance with the Guide for the Care and Use of Laboratory Animals (U.S. National Institutes of Health).

## Immunohistochemistry

Mouse embryos and neonates were collected, fixed in 4% PFA, embedded in OCT, and frozen in dry iced hexane. Frozen sections were blocked with 5% goat serum, stained with mouse anti-TNNT2 (Thermo Scientific), mouse anti-sarcomeric alpha-actinin (Sigma Aldrich), rabbit anti-TNNI3 (Santa Cruz), rabbit anti-TGFβ1 (Abcam), rabbit anti-Ki67 (Thermo Scientific), rabbit anti-phospho-Histone H3 (Cell Signaling Technology), and Hoechst 33342, and visualized using Alexa Fluor-conjugated secondary antibodies (Life Technologies). Image acquisition was performed on a Zeiss LSM510 Meta inverted confocal microscope (Carl Zeiss) or an Eclipse 80i fluorescent microscope (Nikon). Transgenes were detected by PCR from yolk sac DNA of embryos or tail DNA of neonatal pups. For human heart tissues, formalin-fixed paraffin embedded tissue-sections were rehydrated and autoclaved with Citrate Buffer, pH 6.0 (Sigma-Aldrich) and stained with rabbit anti-phospho-Smad2 (EMD Millipore), rabbit anti-PRDM16 (Abcam), mouse anti-sarcomeric alpha-actinin (Sigma Aldrich) and Hoechst 33342, and visualized using Alexa Fluor-conjugated secondary antibodies (Life Technologies). Image acquisition was performed on an Eclipse 80i fluorescent microscope (Nikon). A detailed list of antibodies used is shown in Supplementary Table 10.

## Exome sequencing in case-parent trio

Exome sequencing was performed on patient and both parents using the Agilent SureSelectXT HumanAllExon V4 (50 Mb) (Agilent Technologies). Briefly, 3 μg of genomic DNA was sheared in 130 μl of low TE buffer to a peak size of 150–200 bp using Covaris E220, and then purified with AmpPure XP beads to remove fragments less than 100 bp. The purified DNA fragments were then subjected to Agilent SureSelect Library preparation Kit, ILM, to be end-repaired, A-tailed, and ligated to indexing-specific paired-end adaptor. The adapter-ligated libraries were amplified for five cycles using Herculase II (Agilent Technologies). Amplified Pre-capture libraries (750 ng) were concentrated in 3 μl and hybridized to the target specific baits (SureSelectXT Human All Exon V4; Agilent Technologies) according to the manufacturer's recommendations. Hybridized material was captured using streptavidin-coated beads (Invitrogen, Paisley, UK) and amplified for 10 cycles. Captured libraries were pooled in pairs and paired-end sequenced on one lane of the Illumina HiSeq 2000 at the Stanford Center for Genomics and Personalized Medicine.

## Exome-sequencing data analysis

For each exome, raw reads in FASTQ format were aligned to hg19 using the Burrows-Wheeler aligner (BWA, http://bio-bwa.sourceforge.net/) to produce a BAM (binary alignment/map) file. For case and each parent, approximately 12 Gb high quality mappable data were obtained with an average read coverage of 178X, and 90% of bases in the captured region covered more than 49X. SBgenomics BWA-GATK- and Ingenuity Variant Calling platforms version 2.0.20130604 were used to identify potentially pathogenic variants associated to LVNC. An initial variant dataset (in variant call format, VCF) was generated for each sample using SBgenomics BWA+GATK+Coverage Exome Analysis pipeline. Variants filtering were done based on quality, allele frequency in known populations, pathological potential, genetic analysis, and biological relevance. The initial variant list that contains 2160040 variants, affecting 19706 genes, was filtered for high confidence variants that met the following quality control: (i) SNPs and Indels with overall quality more than 20 and (ii) variants with read depth greater than 10. The "usual suspect" genes were excluded by only keeping variants both outside top 0.2% of most exonically variable 100 base windows and 1% of most exonically variable gene in the 1000 Genomes Project (the database of healthy public genomes; http://www.1000genomes.org/home). To obtain more possible pathogenic variants, low-frequency variants with an allele frequency of more than 0.1% in the databases of 1000 Genomes Project, public Complete Genomics genomes (http://www.completegenomics.com/public-data/) and NHLBI ESP exomes (http://evs.gs.washington.edu/EVS/) were excluded. In addition, suspicious mutations were selected with a focus on suspicious genetic causes that were associated with pathogenic, likely pathogenic, and uncertain significance phenotype. These selected genes have sequence variants associated with 1) non-synonymous mutations including gain of function, loss of function, frame shift, in-frame in-del, start/stop codon change missense which were not tolerated by SIFT or PolyPhen-2, or 2) nucleotide changes in microRNA, or 3) nucleotide changes in likely splice site loss up to 2 bases into intron and structural changes. Finally, 102 variants affecting 108 genes were listed by applying a genetic filtering that selected the genotype occurring in at least 2 out of the 3 case samples and not in control samples, as well as by using a biological filtering that kept only variants known to be implicated in LVNC phenotype within 1 hop upstream. Analyzed data access URL: https://variants.ingenuity.com/Jahanbani2016. Raw data can be accessed as the SRA reference SRP080041.

## Genotyping of LVNC patients

The genotype of each family member was determined by isolating genomic DNA from ~$5\times10^6$ human fibroblasts or PBMCs, using the DNeasy Blood & Tissue kit (Qiagen) according to the manufacturer's instructions. PCR and direct-sequencing was performed as described previously[51]. A detailed list of primers used is shown in Supplementary Table 11.

## shRNA-mediated knockdown

Knockdown of TBX20 was performed using GIPZ Lentiviral Human TBX20 shRNA (V2LHS_286836) and GIPZ Non-silencing Lentiviral shRNA Control (GE Healthcare

Dharmacon) according to the manufacturer's protocol. Knockdown efficiency was measured by qRT-PCR.

### siRNA-mediated knockdown

Gene knockdown experiments were performed using Lipofectamine RNAiMax (Life Technologies) according to manufacturer's instructions. Cells were transfected with either scrambled or siRNA against p21 (Life Technologies; siRNA s415; Ambion Silencer Select, 25 nM/well) for 36 h before being subjected to subsequent downstream analysis.

### Adenoviral mediated dominant negative form of TGFβRII overexpression

The HEK293T cells were purchased from Thermo Fisher Scientific. The cells were not authenticated or tested for mycoplasma contamination recently. No cell lines used in this study were found in the database of commonly misidentified cell lines that is maintained by ICLAC and NCBI Biosample. For adenoviral vector production, ~80% confluent HEK293T cells were transfected for 48 h with an adenovirus expressing a dominant-negative TGFβ type II receptor[52] or eGFP adenovirus (Vector biolabs). The collected supernatants were used for the second transduction to concentrate the virus titer. Titers were measured by using Adeno-X™ qPCR Titration Kit (Clontech). $1\times10^4$ of LVNC iPSC-CMs were transducted with concentrated viral supernatant containing $2.5\times10^4$ transducing particles and incubated for 24 h.

### Treatment with TGFβ receptor-1 inhibitors

TGFβ receptor-1 inhibitors (SD208, RepSox: Selleckchem) were dissolved in DMSO. An equal concentration of solvent (DMSO) was used as control. Both iPSC-CMs and ESC-CMs were treated with SD208 or RepSox for 48 h prior to experiment.

### CRISPR/Cas9-mediated genome editing

CRISPR/Cas9-mediated genome editing was performed as previously described[53]. Single-guide DNA oligonucleotides were subcloned into vector PX458 (Addgene), and were delivered into control iPSCs by nucleofection using P3 Primary Cell 4D-Nucleofector X Kit (Lonza). After 48 h following nucleofection, transfected cells were enriched by fluorescence-activated cell sorting, and established clones were genotyped by PCR and bidirectional direct sequencing.

### Transcription activator-like effector nuclease (TALEN)-mediated genome editing

TALEN pair vectors were designed and constructed using the rapid TALEN assembly system as previously described[54]. 500 bp fragments of wild-type *TBX20* exon 7 and adjacent intronic sequences were synthesized as GeneArt String DNA fragments (Life Technologies) to make left and right homologous arms, and cloned into PB-MV1Puro-TK vector (Transposagen), as previously described[55]. Four silent mutations in homologous arms were inserted in order to create an artificial TTAA site and to avoid re-cleavage of the genomic sequence. Both TALEN pair and targeting vectors were delivered into LVNC iPSCs by nucleofection using P3 Primary Cell 4D-Nucleofector X Kit (Lonza). Afterwards, cells with correct targeting vector integration were selected by puromycin (Life Technologies)

and genotyped. To excise the selection cassette, the transient expression of *piggyBac* transposase was performed by nucleofection of excision-only *piggyBac* transposase plasmid, PBx (Transposagen). After negative selection using ganciclovir (Sigma Aldrich), the established clones were genotyped by PCR and bidirectional direct sequencing.

### Statistics and reproducibility

The experiments were not randomized and no statistical method was used to predetermine sample size. No inclusion/exclusion criteria was applied to the animal study. The investigators were not blinded to allocation during experiments and outcome assessment and replicate experiments were performed on the basis of the severity and variability of phenotypes obtained. Data were expressed as mean ± s.e.m. Immunoblots shown are representative of at least two independent experiments. All other experiments are average of at least two independent assays, and for cell number calculation in immunostaining assays, at least 100 cells per sample were counted for each independent experiments. To confirm the reproducibility, in vitro experiments were performed by two independent operators. Statistical analyses were performed using SPSS statistics 21 software (IBM). An unpaired two-tailed Student's t-test was used to calculate significant differences between two groups. Multiple comparison correction analysis was performed using ANOVA followed by Tukey's Post Hoc HSD test. A $p$-value of $<0.05$ was considered statistically significant. For RNA-sequencing, raw p values were adjusted for multiple testing with the Benjamini-Hochberg procedure. Genes with adjusted p value of 0.05 or less were termed as differentially expressed genes. The investigators were not blinded to allocation during experiments and outcome assessment. Source data is provided in Supplementary Table 12.

### Data availability

Primary RNA-seq data-sets have been deposited in the Gene Expression Omnibus (GEO) under accession code GSE63161. The Exome-sequencing processed data can be accessed on https://variants.ingenuity.com/Jahanbani2016 and raw data can be accessed as the SRA reference SRP080041. Source data for Figures 1–7 and Supplementary Figures 1–5 have been provided in Supplementary Table 12. All other data supporting the findings of this study are available from the corresponding author upon reasonable request.

## Supplementary Material

Refer to Web version on PubMed Central for supplementary material.

## Acknowledgments

We thank Ning Sun, Shijun Hu, and Jaecheol Lee for their help with functional assessments; Hiroyuki Yamagishi for providing plasmid; Adam B. Glick for providing dominant negative TGFB1RII overexpression adeno virus; Bruno Huber, Bhagat Patlolla and Gerald Berry for their help with analyzing *in vivo* study. We are grateful for the support provided by the Neuroscience Microscopy Service (NMS), and FACS Core at the Institute for Stem Cell Biology and Regenerative Medicine, Stanford University. This work is supported by the Uehara Memorial Foundation Research Fellowship, American Heart Association Postdoctoral Fellowship 15POST25160016 (KK), American Heart Association Postdoctoral Fellowship 15POST22940013 and NIH K99HL130416 (SO), The Ministry of Education, Culture, Sports, Science and Technology in Japan (FI), National Institutes of Health P01 GM099130 (MPS), NIH K18 HL11708301, Children's Cardiomyopathy Foundation (DB), AHA Established Investigator Award, NIH R01 HL113006, NIH R01 HL130020, NIH R01 126527, NIH R01 128170, NIH R01 HL123968, and NIH R24 HL117756 (JCW).

## References


1. Kohli SK, et al. Diagnosis of left-ventricular non-compaction in patients with left-ventricular systolic dysfunction: time for a reappraisal of diagnostic criteria? Eur Heart J. 2008; 29:89–95. [PubMed: 17993472]
2. Nugent AW, et al. The epidemiology of childhood cardiomyopathy in Australia. The N Engl J Med. 2003; 348:1639–1646. [PubMed: 12711738]
3. Sedmera D, Pexieder T, Vuillemin M, Thompson RP, Anderson RH. Developmental patterning of the myocardium. Anat Rec. 2000; 258:319–337. [PubMed: 10737851]
4. Chin TK, Perloff JK, Williams RG, Jue K, Mohrmann R. Isolated noncompaction of left ventricular myocardium. A study of eight cases. Circulation. 1990; 82:507–513. [PubMed: 2372897]
5. Kosaka Y, et al. 14-3-3epsilon plays a role in cardiac ventricular compaction by regulating the cardiomyocyte cell cycle. Mol Cell Biol. 2012; 32:5089–5102. [PubMed: 23071090]
6. Chen Q, et al. Smad7 is required for the development and function of the heart. J Biol Chem. 2009; 284:292–300. [PubMed: 18952608]
7. DiMichele LA, et al. Transient expression of FRNK reveals stage-specific requirement for focal adhesion kinase activity in cardiac growth. Circ Res. 2009; 104:1201–1208. [PubMed: 19372463]
8. Bartram U, et al. Double-Outlet Right Ventricle and Overriding Tricuspid Valve Reflect Disturbances of Looping, Myocardialization, Endocardial Cushion Differentiation, and Apoptosis in TGF- 2-Knockout Mice. Circulation. 2001; 103:2745–2752. [PubMed: 11390347]
9. Shou W, et al. Cardiac defects and altered ryanodine receptor function in mice lacking FKBP12. Nature. 1998; 391:489–492. [PubMed: 9461216]
10. Grego-Bessa J, et al. Notch signaling is essential for ventricular chamber development. Dev Cell. 2007; 12:415–429. [PubMed: 17336907]
11. Luxan G, et al. Mutations in the NOTCH pathway regulator MIB1 cause left ventricular noncompaction cardiomyopathy. Nat Med. 2013; 19:193–201. [PubMed: 23314057]
12. Arndt AK, et al. Fine mapping of the 1p36 deletion syndrome identifies mutation of PRDM16 as a cause of cardiomyopathy. Am J Hum Genet. 2013; 93:67–77. [PubMed: 23768516]
13. Chakraborty S, Yutzey KE. Tbx20 regulation of cardiac cell proliferation and lineage specialization during embryonic and fetal development in vivo. Dev Biol. 2012; 363:234–246. [PubMed: 22226977]
14. Takeuchi JK, et al. Tbx20 dose-dependently regulates transcription factor networks required for mouse heart and motoneuron development. Development. 2005; 132:2463–2474. [PubMed: 15843409]
15. Hammer S, et al. Characterization of TBX20 in human hearts and its regulation by TFAP2. J Cell Biochem. 2008; 104:1022–1033. [PubMed: 18275040]
16. Posch MG, et al. A gain-of-function TBX20 mutation causes congenital atrial septal defects, patent foramen ovale and cardiac valve defects. J Med Genet. 2010; 47:230–235. [PubMed: 19762328]
17. Liu C, et al. T-box transcription factor TBX20 mutations in Chinese patients with congenital heart disease. Eur J Med Genet. 2008; 51:580–587. [PubMed: 18834961]
18. Qian L, et al. Transcription factor neuromancer/TBX20 is required for cardiac function in Drosophila with implications for human heart disease. Proc Natl Acad Sci U S A. 2008; 105:19833–19838. [PubMed: 19074289]
19. Kirk EP, et al. Mutations in cardiac T-box factor gene TBX20 are associated with diverse cardiac pathologies, including defects of septation and valvulogenesis and cardiomyopathy. Am J Hum Genet. 2007; 81:280–291. [PubMed: 17668378]
20. Chen G, et al. Chemically defined conditions for human iPSC derivation and culture. Nat Methods. 2011; 8:424–429. [PubMed: 21478862]
21. Churko JM, Burridge PW, Wu JC. Generation of human iPSCs from human peripheral blood mononuclear cells using non-integrative Sendai virus in chemically defined conditions. Methods Mol Biol. 2013; 1036:81–88. [PubMed: 23807788]
22. Burridge PW, et al. Chemically defined generation of human cardiomyocytes. Nat Methods. 2014; 11:855–860. [PubMed: 24930130]

23. Wu H, et al. Epigenetic Regulation of Phosphodiesterases 2A and 3A Underlies Compromised beta-Adrenergic Signaling in an iPSC Model of Dilated Cardiomyopathy. Cell Stem Cell. 2015; 17:89–100. [PubMed: 26095046]
24. D'Amato G, et al. Sequential Notch activation regulates ventricular chamber development. Nat Cell Biol. 2016; 18:7–20. [PubMed: 26641715]
25. Engelmann GL, Boehm KD, Birchenall-Roberts MC, Ruscetti FW. Transforming growth factor-beta 1 in heart development. Mech Dev. 1992; 38:85–97. [PubMed: 1419851]
26. Kitamura R, et al. Stage-specific role of endogenous Smad2 activation in cardiomyogenesis of embryonic stem cells. Circ Res. 2007; 101:78–87. [PubMed: 17540976]
27. Hauck L, et al. Critical role for FoxO3a-dependent regulation of p21CIP1/WAF1 in response to statin signaling in cardiac myocytes. Circ Res. 2007; 100:50–60. [PubMed: 17158337]
28. Akli S, Zhan S, Abdellatif M, Schneider MD. E1A Can Provoke G1 Exit That Is Refractory to p21 and Independent of Activating Cdk2. Circ Res. 1999; 85:319–328. [PubMed: 10455060]
29. Brooks G, Poolman RA, Li JM. Arresting developments in the cardiac myocyte cell cycle: role of cyclin-dependent kinase inhibitors. Cardiovasc Res. 1998; 39:301–311. [PubMed: 9798515]
30. Madisen L, et al. A robust and high-throughput Cre reporting and characterization system for the whole mouse brain. Nat Neurosci. 2010; 13:133–140. [PubMed: 20023653]
31. Sakabe NJ, et al. Dual transcriptional activator and repressor roles of TBX20 regulate adult cardiac structure and function. Hum Mol Genet. 2012; 21:2194–2204. [PubMed: 22328084]
32. Sun N, et al. Patient-specific induced pluripotent stem cells as a model for familial dilated cardiomyopathy. Sci Transl Med. 2012; 4:130ra147.
33. Davis J, et al. A Tension-Based Model Distinguishes Hypertrophic versus Dilated Cardiomyopathy. Cell. 2016; 165:1147–1159. [PubMed: 27114035]
34. Lan F, et al. Abnormal calcium handling properties underlie familial hypertrophic cardiomyopathy pathology in patient-specific induced pluripotent stem cells. Cell Stem Cell. 2013; 12:101–113. [PubMed: 23290139]
35. Hinson JT, et al. Titin mutations in iPS cells define sarcomere insufficiency as a cause of dilated cardiomyopathy. Science. 2015; 349:982–986. [PubMed: 26315439]
36. Moretti A, et al. Patient-specific induced pluripotent stem-cell models for long-QT syndrome. N Engl J Med. 2010; 363:1397–1409. [PubMed: 20660394]
37. Itzhaki I, et al. Modelling the long QT syndrome with induced pluripotent stem cells. Nature. 2011; 471:225–229. [PubMed: 21240260]
38. Wang Y, et al. Genome editing of isogenic human induced pluripotent stem cells recapitulates long QT phenotype for drug testing. J Am Coll Cardiol. 2014; 64:451–459. [PubMed: 25082577]
39. Matsa E, Ahrens JH, Wu JC. Human Induced Pluripotent Stem Cells as a Platform for Personalized and Precision Cardiovascular Medicine. Physiol Rev. 2016; 96:1093–1126. [PubMed: 27335446]
40. Takahata M, et al. SKI and MEL1 cooperate to inhibit transforming growth factor-beta signal in gastric cancer cells. J Biol Chem. 2009; 284:3334–3344. [PubMed: 19049980]
41. Warner DR, et al. PRDM16/MEL1: a novel Smad binding protein expressed in murine embryonic orofacial tissue. Biochim Biophys Acta. 2007; 1773:814–820. [PubMed: 17467076]
42. Bjork BC, Turbe-Doan A, Prysak M, Herron BJ, Beier DR. Prdm16 is required for normal palatogenesis in mice. Hum Mol Genet. 2010; 19:774–789. [PubMed: 20007998]
43. Oechslin E, Jenni R. Left ventricular non-compaction revisited: a distinct phenotype with genetic heterogeneity? Eur Heart J. 2011; 32:1446–1456. [PubMed: 21285074]
44. Sen-Chowdhry S, McKenna WJ. Left ventricular noncompaction and cardiomyopathy: cause, contributor, or epiphenomenon? Curr Opin Cardiol. 2008; 23:171–175. [PubMed: 18382203]
45. Kodo K, et al. GATA6 mutations cause human cardiac outflow tract defects by disrupting semaphorin-plexin signaling. Proc Natl Acad Sci U S A. 2009; 106:13933–13938. [PubMed: 19666519]
46. Stevenson KR, Coolon JD, Wittkopp PJ. Sources of bias in measures of allele-specific expression derived from RNA-sequence data aligned to a single reference genome. BMC Genomics. 2013; 14:536. [PubMed: 23919664]

47. Abel ED, et al. Cardiac hypertrophy with preserved contractile function after selective deletion of GLUT4 from the heart. J Clin Invest. 1999; 104:1703–1714. [PubMed: 10606624]

48. Muzumdar MD, Tasic B, Miyamichi K, Li L, Luo L. A global double-fluorescent Cre reporter mouse. Genesis. 2007; 45:593–605. [PubMed: 17868096]

49. Chen WP, Liu YH, Ho YJ, Wu SM. Pharmacological inhibition of TGFbeta receptor improves Nkx2.5 cardiomyoblast-mediated regeneration. Cardiovasc Res. 2015; 105:44–54. [PubMed: 25362681]

50. Hall BE, et al. Conditional overexpression of TGF-beta1 disrupts mouse salivary gland development and function. Lab Invest. 2010; 90:543–555. [PubMed: 20142803]

51. Chang B, et al. 14-3-3epsilon gene variants in a Japanese patient with left ventricular noncompaction and hypoplasia of the corpus callosum. Gene. 2013; 515:173–180. [PubMed: 23266643]

52. Markell LM, Masiuk KE, Blazanin N, Glick AB. Pharmacologic inhibition of ALK5 causes selective induction of terminal differentiation in mouse keratinocytes expressing oncogenic HRAS. Mol Cancer Res. 2011; 9:746–756. [PubMed: 21521744]

53. Ran FA, et al. Genome engineering using the CRISPR-Cas9 system. Nat Protoc. 2013; 8:2281–2308. [PubMed: 24157548]

54. Ding Q, et al. A TALEN genome-editing system for generating human stem cell-based disease models. Cell Stem Cell. 2013; 12:238–251. [PubMed: 23246482]

55. Yusa K. Seamless genome editing in human pluripotent stem cells using custom endonuclease-based gene targeting and the piggyBac transposon. Nat Protoc. 2013; 8:2061–2078. [PubMed: 24071911]

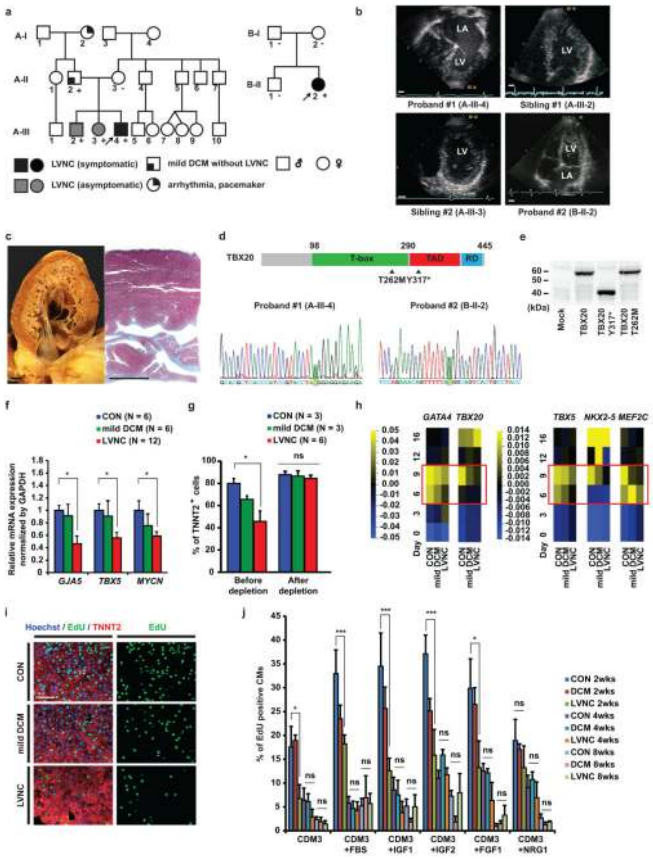

**Figure 1. Characterization of patient-specific LVNC iPSC-CMs carrying TBX20 mutation**

**a**, Schematic pedigree of two families with LVNC. The probands are indicated by arrow (A-III-4 and B-II-2). "+" and "−" signs indicate presence and absence of the TBX20 Y317* mutation in the family A and T262M mutation in the family B, respectively. **b**, LVNC phenotype of the proband #1 (A-III-4), two siblings (A-III-2 and A-III-3), and an isolated proband #2 (B-II-2) are assessed by echocardiography. LA, left atrium; LV, left ventricle. Scale bars, 1 cm. **c**, The proband #1's explanted heart (left) and Masson's trichrome staining of the left ventricle (right). Scale bars, 1 cm. **d**, Schema of TBX20 and position of Y317* and T262M mutations (Upper). Confirmation of the Y317* (c. 951C>A) and T262M (c. 785C>T) mutation on the TBX20 gene (highlighted in green) (Lower). TAD, transactivation domain; RD repression domain. **e**, Western blot of FLAG tagged wild-type, Y317* and T262M TBX20 mutant protein overexpressed in HEK293 cells. **f**, Significant downregulation of TBX20 downstream target gene mRNA expression in LVNC iPSC-CMs. **g**, The efficiency of cardiac differentiation of patient-specific iPSC lines validated by FACS sorting. **h**, Heat map showed mRNA expression of cardiac transcription factors in iPSCs from day 0 to day 16 after induction of cardiac differentiation. The LVNC iPSCs showed significant decrease of cardiac transcription factors in day 6 and day 9 (red boxes). n=6 independent experiments. Mean=0. **i**, Immunostaining of nuclear (blue), TNNT2 (red), and EdU (green) in iPSC-CMs at 2 weeks. Scale bars, 100 μm. **j**, Percentage of EdU$^{+}$ cardiomyocytes in control, mild DCM, and LVNC iPSC-CMs with or without serum (n=10, 10 and 30 for CON, mild DCM and LVNC independent experiments respectively at 2

weeks; n=4 independent experiments per each group at 4 and 8 weeks) or with growth factors (n=4 independent experiments per each group at 2, 4, and 8 weeks). CON, unrelated controls. *$p < 0.05$, ***$p < 0.005$; ns, not significant in one-way ANOVA followed by Tukey post hoc test. The bar graphs show the mean and error bars represent s.e.m. Statistics source data can be found in Supplementary Table 12. Unprocessed original scans of blots are shown in Supplementary Fig. 8.

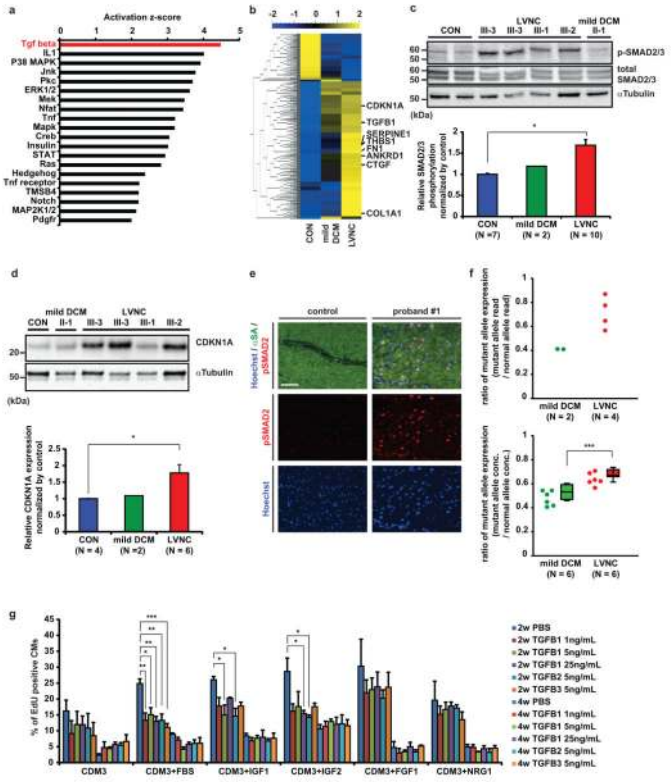

**Figure 2. Upregulation of TGFβ signaling in LVNC phenotype**

**a**, Upstream regulator analysis of signaling pathway comparing LVNC and control iPSC-CMs at 2 weeks after induction of cardiac differentiation. The *p*-value measures whether there is a statistically significant overlap between the dataset genes and the genes that are regulated by a transcription regulator. **b**, Heat map showing upregulation of TGFβ signaling pathway in LVNC (III-2, 3, 4; mean of four samples) and mild DCM (II-2; mean of two samples) compared to control iPSC-CMs (unrelated controls; mean of two samples). Mean=0, variance=1. **c**, Western blot of total and phospho-SMAD2/3 in control and patient-specific iPSC-CMs (upper) and densitometry analysis, normalized against α-tubulin (lower). **d**, Western blot of CDKN1A protein in control and patient-specific iPSC-CMs (upper) and densitometry analysis, normalized against α-tubulin (lower). **e**, Immunostaining of nuclear (blue), alpha-sarcomeric actin (green), and phospho-SMAD2 (red) in LV of control donor heart tissue vs. explanted heart of proband #1. **f**, Allele-specific mRNA expression analysis by mRNA-sequencing (upper panel) and digital droplet PCR (lower panel) showed a higher ratio of *TBX20* mutant allele expression in LVNC iPSC-CMs compared to mild DCM iPSC-CMs. n=6 independent experiments. **g**, The effect of TGFβ isoform treatments on the percentage of $EdU^+$ cardiomyocytes in control iPSC-CMs with or without growth factors. PBS treated control; n = 4 independent experiments, TGFβ treated samples; n = 3 independent experiments. CON, unrelated controls. $*p < 0.05$, $**p < 0.01$, $***p < 0.005$ in unpaired two-tailed *t*-test or one-way ANOVA followed by Tukey post hoc test. The bar graphs show the mean and error bars represent s.e.m. Scale bars, 100 μm. Statistics source data can be found in Supplementary Table 12. Unprocessed original scans of blots are shown in Supplementary Fig. 8.

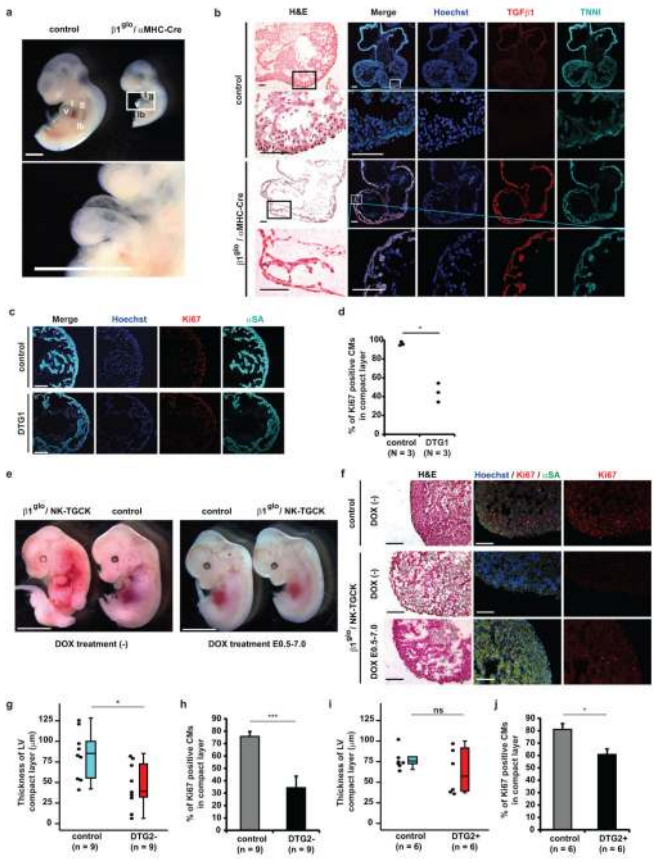

**Figure 3. Developmental arrest in cardiomyocyte-specific TGFβ1 overexpression mouse embryo heart**

**a**, Lateral view of double transgenic embryo (β1$^{glo}$/αMHC-Cre) at embryonic day (E) 10.5 compared to wild-type littermate (control). The lower panel shows higher magnification view of the double transgenic embryo heart (white box in upper panel). Scale bars, 1 mm. **b**, Hematoxylin and eosin (H&E) staining and immunostaining of nuclear (blue), Ki67 (red), and αSA (cyan) in control and β1$^{glo}$/αMHC-Cre double transgenic (DTG1) embryo hearts at E10.5. Scale bars, 100 μm. **c,** Immunostaining for nuclear (blue), TGFβ1 (red), and TNNI (cyan) in coronal sections of control and DTG1 hearts at E10.5. Higher magnification pictures of compact layer (indicated by white box in upper panels) are shown in lower lane. Scale bars, 100 μm. **d**, Percentage of Ki67$^{+}$ cardiomyocytes in compact layer of control and DTG1 embryo hearts at E10.5. **e,** The systemic phenotypes of partially TGFβ1-overexpressed double transgenic embryo (β1$^{glo}$/NE-TGCK) at E12.5 compared to wild-type littermate (control) with or without doxycycline (DOX) treatment. Scale bars, 5 mm. **f,** H&E and immunostaining of nuclear (blue), Ki67 (red), and αSA (cyan) in wild-type (control) and β1$^{glo}$/NE-TGCK double transgenic embryo hearts at E12.5. Scale bars, 100 μm. **g,** Dot and box plot of thickness of left ventricle (LV) compact layer in control and β1$^{glo}$/NE-TGCK double transgenic embryo (DTG2−) hearts without DOX treatment at E12.5. **h,** DTG2− embryo hearts showed significant decrease of percentage of Ki67$^{+}$ cardiomyocytes in compact layer at E12.5. **i,** Dot and box plot of thickness of left ventricle (LV) compact layer in control and DOX-treated β1$^{glo}$/NE-TGCK double transgenic embryo (DTG2+)

hearts at E12.5. **j,** DTG2+ embryo hearts showed significant decrease of percentage of Ki67$^{+}$ cardiomyocytes in compact layer at E12.5. v, ventricle; I, 1$^{st}$ pharyngeal arch; II, 2$^{nd}$ pharyngeal arch; lb, limb bud. *$p < 0.05$, ***$p < 0.005$; ns, not significant in unpaired two-tailed *t*-test. The bar graphs show the mean and error bars represent s.e.m. The box plot shows the median, with upper and lower percentiles, and the bars show maxima and minima values. Statistics source data can be found in Supplementary Table 12.

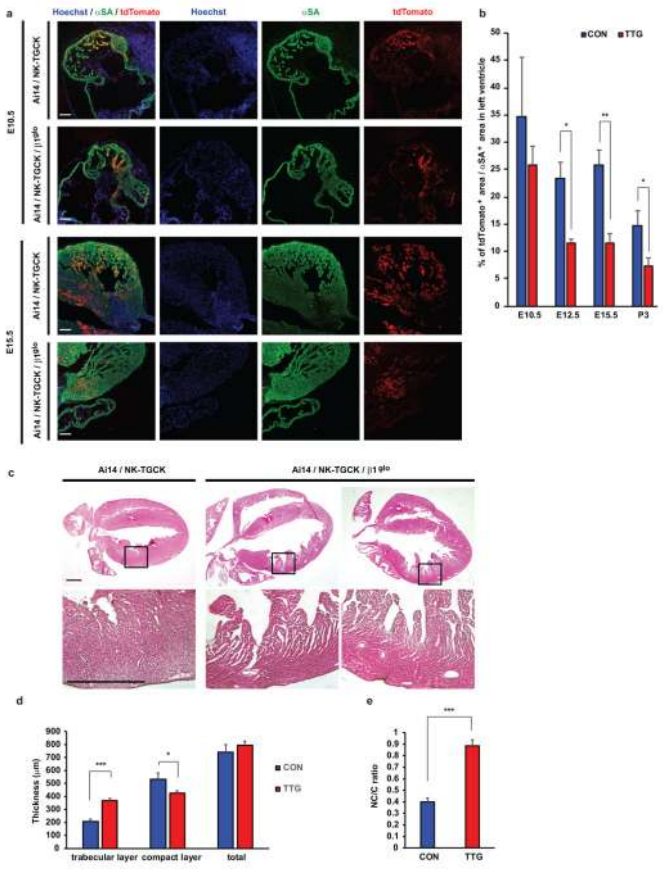


**Figure 4. Disturbed expansion of embryonic cardiomyocytes and trabecular/compact layer ratio in left ventricle of TGFβ1-overexpression mouse**

**a**, Immunostaining of nuclear (blue), tdTomato (red), and αSA (green) in coronal sections of control (Ai14/NK-TGCK) and Ai14/NK-TGCK/β1$^{glo}$ triple transgenic embryo hearts with doxycycline treatment at E10.5 and E15.5. Scale bars, 100 μm. b, Percentage of tdTomato positive area per αSA positive area in compact layer of control and Ai14/NK-TGCK/β1$^{glo}$ triple double transgenic mouse hearts with doxycycline treatment at E10.5 (control; n=5 hearts, triple transgenic; n=5 hearts), E12.5 (control; n=6 hearts, triple transgenic; n=5 hearts), E15.5 (control; n=6 hearts, triple transgenic; n=5 hearts), and postnatal day 3 (P3) (control; n=18 hearts, triple transgenic; n=8 hearts). c, Hematoxylin and eosin staining in coronal sections of control (CON: Ai14/NK-TGCK) and Ai14/NK-TGCK/β1$^{glo}$ triple double transgenic mouse (TTG) hearts with doxycycline treatment at postnatal day (P) 3. Lower panels show hyper-magnified views of areas indicated by the black box in the upper panels. d, Thickness of trabecular and compact layer and total myocardium in control (n=8 hearts) and Ai14/NK-TGCK/β1$^{glo}$ triple transgenic mouse (n=11 hearts) hearts with doxycycline treatment at P3. e, Trabecular layer/compact layer (NC/C) ratio in control (n=8 hearts) and Ai14/NK-TGCK/β1$^{glo}$ triple transgenic mouse hearts (n=11 hearts) with doxycycline treatment at P3. Scale bars, 0.5 mm. *$p < 0.05$, **$p < 0.01$, ***$p < 0.005$ in unpaired two-tailed *t*-test. The bar graphs show the mean and error bars represent s.e.m. Statistics source data can be found in Supplementary Table 12.

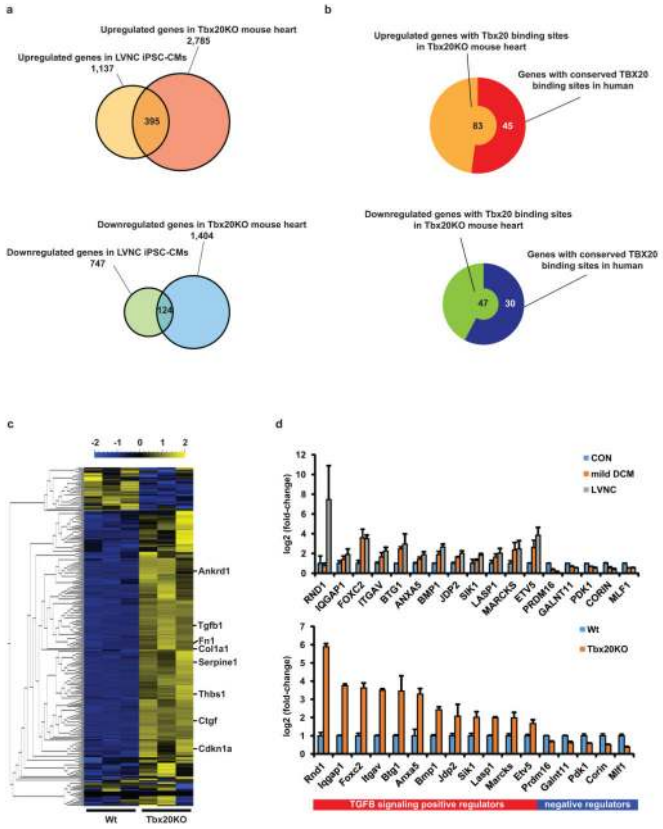


**Figure 5. TBX20 regulates the expression of TGFβ signaling modifier genes in developing cardiomyocytes**

**a**, Venn diagram to show the overlap between genes upregulated (upper) or downregulated (lower) in LVNC iPSC-CMs compared to control iPSC-CMs ($q$<0.05), and upregulated (upper) or downregulated (lower) in Tbx20 knockout mouse heart compared to wild type ($q$<0.05). The mouse data were obtained from NCBI GEO database (http://www.ncbi.nlm.nih.gov/geo)[31]. **b**, Predicted number of upregulated (left) or downregulated (right) genes with Tbx20 binding sites in Tbx20KO mouse heart and number of genes with conserved Tbx20 binding site between mouse and human. The ChIP-sequencing data were obtained from NCBI GEO database (http://www.ncbi.nlm.nih.gov/geo/query/acc.cgi?acc=GSM734426). **c**, The heat map of TGFβ signaling pathway showing upregulation of TGFβ signaling pathway in Tbx20 knockout mouse heart compared to wild-type mouse heart. Mean=0, variance=1. **d**, Significant mRNA expression changes of TBX20 downstream target genes that are involved in TGFB signaling pathway as validated by RNA-sequencing. These genes were found to have conserved binding sites in both human (LVNC vs. control iPSC-CMS: upper) and mouse (Tbx20 knockout vs. wild type mouse heart: lower). The bar graphs show the mean and error bars represent s.e.m.

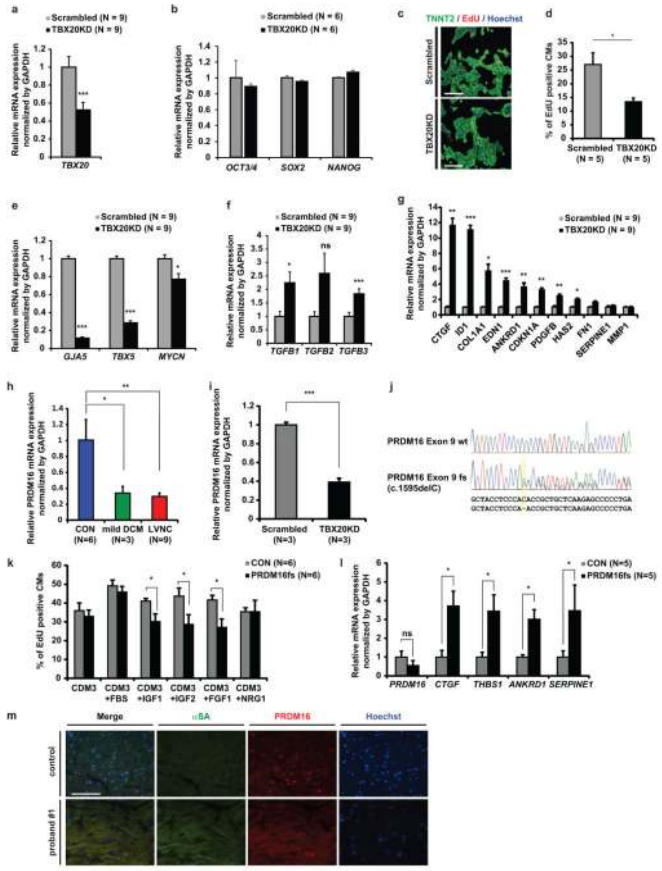

**Figure 6. PRDM16 is a candidate target gene of TBX20 in cardiomyocytes**

**a**, Validation of TBX20 shRNA knockdown efficiency in lentiviral TBX20 shRNA-transduced H7 ESC-CMs (TBX20KD) compared to scrambled shRNA-transduced H7 ESC-CMs (Scrambled) at 2 weeks. n=9 independent experiments per each group. **b**, Validation of pluripotent gene expression profile in TBX20KD and scrambled ESCs by qRT-PCR. **c**, Immunostaining of nuclear (blue), TNNT2 (green), and EdU (red) in scrambled and TBX20KD ESC-CMs at 2 weeks. **d**, Percentage of $EdU^+$ ESC-CMs in scrambled and TBX20KD ESC-CMs at 2 weeks. **e**, Significant decrease of TBX20 downstream target gene (GJA5, TBX5, and MYCN) expressions in TBX20KD ESC-CMs compared to scrambled ESC-CMs at 2 weeks. **f–g** Significant increase of TGFβ isoforms (f) and TGFβ downstream target gene (g) expression in TBX20KD ESC-CMs compared to scrambled ESC-CMs at 2 weeks. **h–i**, Significant decrease of PRDM16 mRNA expression in LVNC iPSC-CMs compared to control iPSC-CMs (h) and in TBX20KD-H7-CMs compared to scrambled H7-CMs (i). **j**, CRISPR/Cas9-based frame shift mutation in exon 9 of PRDM16 gene in control iPSC lines (PRDM16 p.T532fs*8, c.1595delC: highlighted in yellow). **k**, Percentage of $EdU^+$ cardiomyocytes in control and PRDM16 frame shift mutation-created iPSC-CMs (PRDM16fs) with or without growth factors. **l**, Significant increase of TGFβ downstream target gene expressions in PRDM16fs iPSC-CMs. **m**, Immunostaining of nuclear (blue), alpha-sarcomeric actin (green), and PRDM16 (red) in LV of donor's control heart tissue and explanted heart of proband #1. CON, unrelated controls. *$p < 0.05$. **$p < 0.01$. ***$p <$

0.001; ns, not significant in unpaired two-tailed *t*-test or one-way ANOVA followed by Tukey post hoc test. The bar graphs show the mean and error bars represent s.e.m. Scale bars, 100 μm. Statistics source data can be found in Supplementary Table 12.

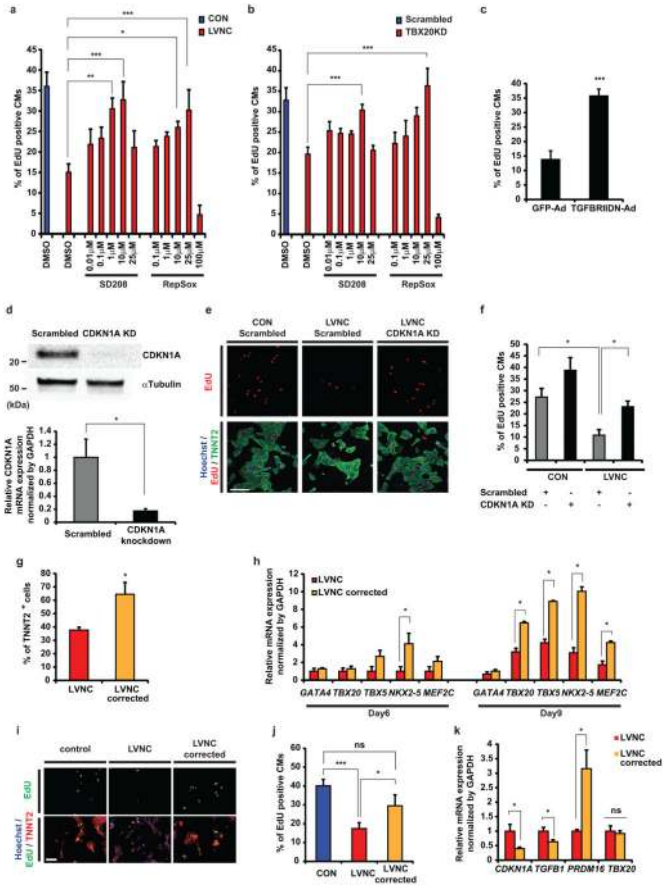

**Figure 7. Rescue of pathological features of LVNC iPSC-CMs**

**a–b**, Percentage of EdU$^+$ control and LVNC iPSC-CMs (a) or scramble control and TBX20 knock-down ESC-CMs (b) at 2 weeks after induction of cardiac differentiation with or without treatment of TGFβ receptor-1 inhibitors (SD208 or RepSox) for 2 continuous days. n=7 independent experiments. **c**, Adenoviral mediated overexpression of dominant negative form of TGFβ receptor-2 (TGFBRIIDN) significantly restored proliferative potential in LVNC iPSC-CMs compared to control (adenoviral mediated GFP overexpression; GFP-Ad). n=8 independent experiments. **d**, Knockdown efficiency of CDKN1A protein (upper) and mRNA (lower) in iPSC-CMs by siRNA. n=6 independent experiments. **e**, Immunostaining for nuclear (blue), TNNT2 (green), and EdU (red) in control and LVNC iPSC-CMs with CDKN1A or scramble siRNA knockdown. **f**, Percentage of EdU$^+$ iPSC-CMs at 2 weeks after induction of cardiac differentiation with CDKN1A or scramble siRNA knockdown. n=6 independent experiments. **g**, The efficiency of cardiac differentiation of LVNC and mutation corrected LVNC iPSC lines before glucose deprivation as validated by FACS for TNNT2. n=5 independent experiments per each group. **h**, mRNA expression of cardiac transcription factors in differentiating LVNC and mutation corrected LVNC iPSCs at day 6 and day 9 after induction of cardiac differentiation. LVNC n=6 independent experiments; LVNC corrected n=5 independent experiments. **i**, Immunostaining for nuclear (blue), TNNT2 (green), and EdU (red) in control, LVNC, and TBX20 mutation corrected (LVNC corrected) iPSC-CMs. **j**, Percentage of EdU$^+$ iPSC-CMs at 2 weeks in control, LVNC, and

LVNC corrected group. n=6 independent experiments. **k**, Reversible CDKN1A, TGFB1, and PRDM16 mRNA expression abnormality in LVNC corrected iPSC-CMs compared to LVNC iPSC-CMs. n=6 independent experiments. CON, unrelated controls. Scale bars, 100 μm. *p < 0.05, **p < 0.01, ***p < 0.005; ns, not significant in unpaired two-tailed *t*-test or one-way ANOVA followed by Tukey post hoc test. The bar graphs show the mean and error bars represent s.e.m. Statistics source data can be found in Supplementary Table 12. Unprocessed original scans of blots are shown in Supplementary Fig. 8.